water

MDPI

Article

Estimation of the Spring Tide Bedload Transport at the Eastern Entrance of the Qiongzhou Strait

Changliang Tong [1,2,3], Maogang Qin [1,3], Xuemu Wang [1,3] and Xiangbai Wu [4,*]

1 Hainan Key Laboratory of Marine Geological Resources and Environment, Haikou 570206, China
2 Hainan Geology Detection and Research Centre, Haikou 570206, China
3 Marine Geological Institute of Hainan Province, Haikou 570206, China
4 School of Naval Architecture and Ocean Engineering, Jiangsu University of Science and Technology, Zhenjiang 212100, China
* Correspondence: xbwu@just.edu.cn

Abstract: Marine sediment deposits near the Qiongzhou Strait have great potential as sources for beach nourishment and infrastructure industry aggregates. Estimation of bedload transport during the spring tide improves the understanding of the sediment movement characteristic under dynamic conditions, which would further favor the assessment and mining of marine sand resources. To study the bedload transport at the eastern entrance of the Qiongzhou Strait, the surficial sediment distributions were obtained through hundreds of sediment samples from field work. A semi-implicit cross-scale hydrological science integrated system model was adopted and validated to simulate the tidal currents in the Qiongzhou Strait. With field observation and simulated data, we estimated the spring tide bedload transport in the study area using the Bagnold Model. The transport rate in the study area was found to have large temporal and spatial variation. The net transport direction during the spring tide cycle was eastward in the southern parts of the strait and westward in the northern strait. Our research has important implications for regional engineering and marine resources management.

Keywords: bedload transport; sediment grain size; SCHISM; Qiongzhou Strait

check for updates

Citation: Tong, C.; Qin, M.; Wang, X.; Wu, X. Estimation of the Spring Tide Bedload Transport at the Eastern Entrance of the Qiongzhou Strait. *Water* **2023**, *15*, 724. https://doi.org/10.3390/w15040724

Academic Editors: Benwei Shi and Aijun Wang

Received: 29 November 2022
Revised: 6 February 2023
Accepted: 9 February 2023
Published: 11 February 2023

1. Introduction

The Qiongzhou Strait is about 25 km wide, connecting the northern part of the South China Sea (SCS) and the Beibu Gulf. At the east entrance of the Qiongzhou Strait, tidal sand ridges develop under the tide-dominated dynamic environment [1–6]. With the local eco-society development of Hainan Island and restriction of river sand mining, there is an increasing demand for marine sand resources [7–12]. The huge sand bodies of the tidal sand ridges have great potential as sources for infrastructure construction, beach nourishment, and ecosystem restoration [13–15].

The formation and evolution of the tidal sand ridges at the eastern entrance of the Qiongzhou Strait have been studied mainly through the analysis of hydrodynamic conditions, geomorphology, and stratigraphic structures [4–6,15]. Cheng et al. [3] examined the long-term bedform instability over the tidal sand ridges with historical nautical charts and seismic profiling. The bedform movement celerity is found to be related to the current velocity, bedform spatial scale, and sediment grainsize. As shown by field observations made at a cross-section in the middle of the strait, the net bedload transportation during spring tide is northeastern, while it shifts to the west during neap tide [3]. The transportation of water mass and sediment is westward near the northern coast, but eastward in the southern part of the strait with much stronger transportation during spring tide than that of neap tide [4]. However, sediment dynamics in the eastern part of the strait have not been comprehensively analyzed with systematic sediment distribution information.

The sediment distribution is closely related to seabed morphology and seabed stability [16,17]. Sediment distribution itself is usually used to distinguish differences in sedimentary environments and to study sediment dynamics [18–22]. The spatial trends of sediment transport can be estimated by sediment grain size trend analysis [12,23–26]. Moreover, in areas where the seabed is covered by coarse sand and gravel, a significant portion of sediments will move as bedload in the more extreme current conditions. Since the bedload responds rapidly to local flow conditions, it is possible that bedload influences the evolution of bed morphology more than suspension does at a local scale [27–29].

The hydrodynamic condition near the Qiongzhou Strait is dominated by strong tidal forcing. Under the action of east-west tidal currents, the sedimentary environment ranges from erosion inside to accumulation outside the strait. Eroded channels have formed inside the strait due to the strong tidal currents. At the outlets of the strait, the slowdown of tide flow reduces its sediment-carrying capacity, which creates finger-like tidal sand ridges [1–3]. At the east entrance of Qiongzhou Strait, surficial sediment is mainly gravel and sand, and bed load and saltation load dominated the sediment transportation [30]. It is important to estimate the bedload transport during spring tide, as it not only decides local sediment redistribution, seabed stability, and seabed morphology, but also influences the assessment and mining of marine sand [31,32].

In recent years, there has been a migration of tropical cyclones toward coasts in global oceans [33]. In the western North Pacific Ocean, tropical cyclones show westward migration, which leads to an increase in the possibility of landfall near the Qiongzhou Strait and adjacent areas. The interactions among tide, surge, and waves during storm events can be significant in shallow waters due to the local enhancement by the complicated bathymetric features and geometric configurations. Further, tide-surge and wave interaction also have significant impact on sediment transport in the littoral zone [34,35]. Although the study of wind-current-wave interaction and tidal surge is beyond the scope of this paper, the present study offers an important reference to the sediment dynamics under such complex dynamic conditions during storm events.

In this paper, we present the distribution of surficial sediment, tidal current during spring tide from both observation and numerical simulation, and sediment transport of the Qiongzhou Strait through the comprehensive analysis of tidal currents and seabed morphology. Our conclusions provide a scientific basis for marine environmental protection and the management of marine resources [36].

2. Materials and Methods

2.1. Overview of the Study Area

The east entrance of the Qiongzhou Strait experienced transgressive and regressive episodes during the Quaternary, leaving a large thickness of sediment in the area. Global sea level rise since the last glacial period created the Qiongzhou Strait, which connected the previously isolated water bodies in the northern SCS and the Beibu Gulf. Due to strong tidal currents, tens of large tidal sand ridges have formed at the outlets of the strait [6,37]. The orientation of the tidal sand ridges is consistent with the main direction of tidal currents. Erosion channels are located between the sand ridges. The sediments in this area are mainly sand and gravel, which gradually become finer from west to east and are fine sand at the far end of the sand ridges [15]. Tides in the study area are irregular semi-diurnal tides, with an average tidal range of 1.42 m. The maximum surface current velocity can reach 1–2 m/s, and the maximum bottom current can reach 1 m/s [5,38,39]. The residual current is westward with a maximum velocity of 10–40 cm/s at the surface [40,41]. The average wave height at the eastern entrance of the strait is 0.9–1.0 m. The normal wave direction and strong wave direction in the study area are NNE [5,42].

2.2. Field Work and Data Processing

The seabed surface sediment samples were collected during two field surveys in 2008 and 2015. A total of 249 stations were sampled, with a sampling interval of about

5 km (locally enhanced sampling over the southern part of the study area, Figure 1). The sampling thickness was 5 cm of the seabed surface. After pre-treatment to remove organic matter, calcium carbonate, and salt, the sediments were dispersed using sodium hexametaphosphate and ultrasonic vibration. For sediments with a particle size of less than 2 mm, a Mastersizer2000 laser particle size analyzer (produced by Malvern, UK) was used for grain size measurement. For coarser sediments, the sieving method was used for grain size analysis. The complete particle size distribution was obtained after normalization. The grain size parameters were calculated using the graphic method. Sediments were classified using the Folk-Ward classification system [23].

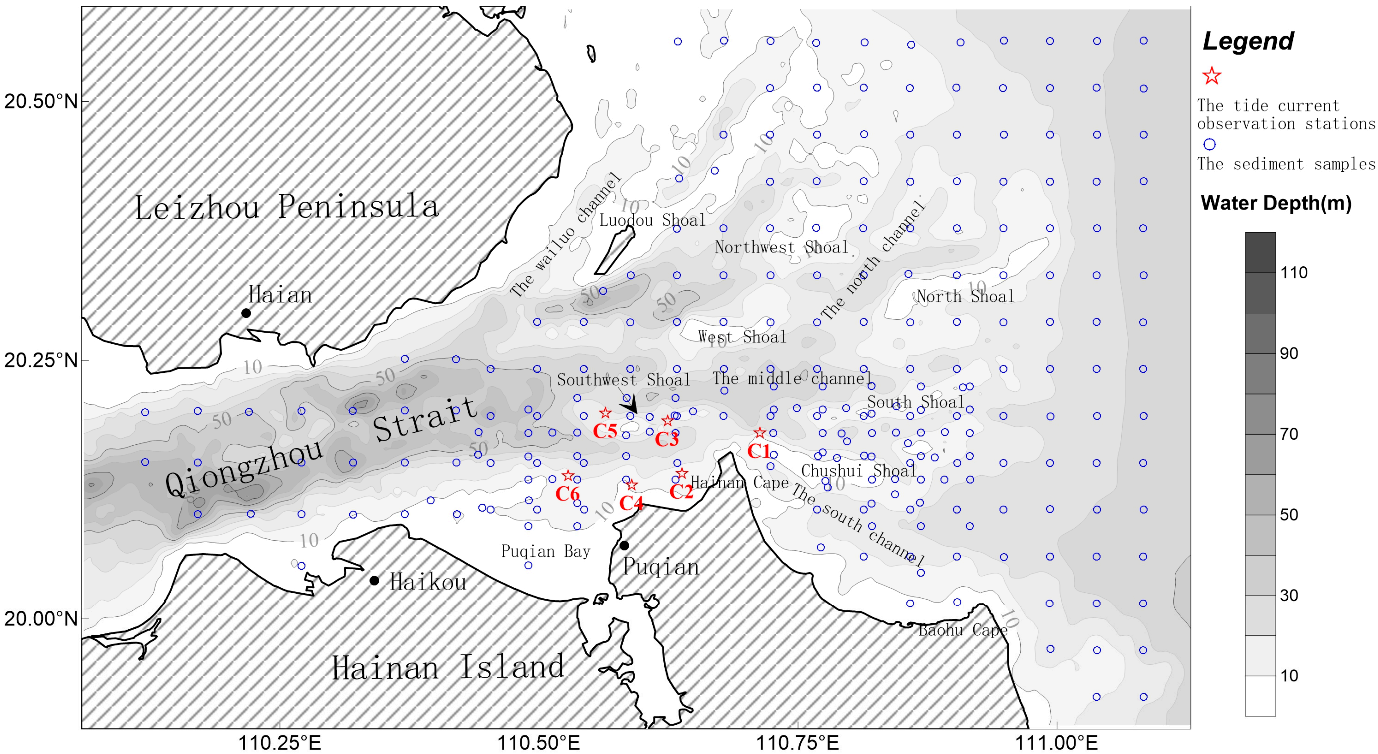

Figure 1. The topography and geomorphology of the east entrance of Qiongzhou Strait. Blue circles denote the seabed sediment sampling stations, Red asterisks denote the six field observation stations for tidal current.

Tidal current observations were collected from 09:00 on 8 March to 10:00 on 9 March 2020 (spring tide) at six stations in the study area. The 25 h tidal current observation was conducted simultaneously at the six stations. Tidal velocity profiles were collected at 1 hr intervals using the three-point method (surface layer, 0.6 h, bottom layer, where h is the depth of the water column). The observation was carried out with the AEM-USB self-recording ocean current meter, the depth-mean velocity was then calculated.

2.3. Numerical Simulation of Tidal Current

The tidal current was simulated through numerical models to examine the characteristics of the tidal current in the study area. Considering the complex terrain near the Qiongzhou Strait, a semi-implicit cross-scale hydrological science integrated system model (SCHISM) with an unstructured triangular grid was adopted. SCHISM is a derivative product built from the original semi-implicit Eulerian-Lagrangian finite-element model (SELFE, v3.1dc; [43]) and distributed with an open-source Apache v2 license, with many enhancements and upgrades, including a new extension to the large-scale eddying regime and a seamless cross-scale capability from creek to ocean [44]. It uses a highly efficient and accurate semi-implicit finite-element/finite-volume method with Eulerian-Lagrangian algorithms to solve the Navier-Stokes equations (in hydrostatic form), in order to addresses a wide range of physical and biological processes. The numerical algorithm judiciously mixes higher-order with lower-order methods, to obtain stable and accurate results in an efficient way. This model has had a relatively stable performance for complex terrain areas and has been widely used in offshore sedimentary dynamics [45,46]. The SCHISM model uses an unstructured horizontal triangular grid covering the northwestern part of the South China Sea (105–113° E, 16–22° N), with a total of 49,221 nodes and 91,827 elements. The bathymetry in the modeling domain is generated from SRTM15+ [47] with a spatial resolution at 15 arc seconds, and regional digital China Nautical Charts published by the Navigation Guarantee Department of the Chinese Navy Headquarters. The mesh resolution ranged from 200 m in the Qiongzhou Strait to 15 km on the open ocean boundary. There are 40 layers in total, with 20 sigma layers at 40 m or shallower water. Z levels of thickness of 5 m to 200 m were adopted for water depths of 40 to 2200 m. The model was verified by the water level time series from the tide gauge stations.

2.4. Calculation of Bedload Transport Rate

The bedload transport rate is calculated using the Bagnold [48] method. Based on the coarser sediment particles in this area, the Hardisty [49] equation is used for calculation as follows:

$$q_b = k_1\left({U_{100}}^2 - {U_{100\ cr}}^2\right)U_{100} \tag{1}$$

where q_b is the bedload transport rate (kg·m^{-1}·s^{-1}), U_{100} is the vector of tidal current velocity 100 cm above the seabed (m·s^{-1}), and $U_{100\ cr}$ is the critical incipient velocity at 100 cm height from the seabed (m·s^{-1}).

U_{100} is converted from depth-mean velocity according to the empirical equation of Soulsby [29,50]. The direction remains the same. The equation is as follows:

$$U_z = \left(\frac{z}{0.32h}\right)^{1/7}\overline{U}, 0 < \mathrm{z} < 0.5\ \mathrm{h}, \tag{2}$$

where z is the height from the seabed (m), h is the water depth (m), and U is the depth-mean velocity (m·s^{-1}).

$U_{100\ cr}$ is a function of sediment grain size. The equation is as follows [51]:

$$U_{100\ cr} = 122.6\ {d_{50}}^{0.29}\mathrm{d} < 0.2\ \mathrm{cm}, \tag{3}$$

where d_{50} is the median grain size of the sediments (cm).

In Equation (1), k_1 is a coefficient with a dimension of kg·m^{-4}·s^{-2}, which is a function related to the grain size of the sediment. That equation is as follows [52,53]:

$$k_1 = 0.10exp\left(\frac{0.17}{d_{50}}\right), \mathrm{d}_{50} > 0.2\ \mathrm{mm}, \tag{4}$$

$$k_1 = \frac{1}{8.9{d_{50}}^{0.42}}, \mathrm{d}_{50} < 0.2\mathrm{mm}. \tag{5}$$

3. Results and Discussion

3.1. Sediment Distribution

Distribution of the grain fraction of the sediment in the study area is shown in Figure 2. The gravel component is mainly located in the western part of the study area, close to the main channel of Qiongzhou Strait. In this area, the gravel constitutes about 20% to 50% of the sediment samples. In other regions, the gravel content is less than 10%. The average gravel content of the entire study area is 9.7%. The dominant grain size in the study area is sand, making up an average of about 71.0% of the sediment samples. The high sand content areas occur mainly among the tidal sand ridges at the east entrance of the strait and also near the estuaries, where the sand content ranges from 40% to 100%. The high-sand area accounts for more than 60% of the study area. In the open continental shelf to the east of the tidal sand ridges, the sand content is also about 10% to 30%. The area with high silt content (between 30% and 70%) is located on the open shelf to the east of the tidal sand ridges and in the bays along Qiongzhou Strait. In other areas, the silt content is generally less than 20%. On average, silt content over the entire area is 15.3%. The average clay content in the study area is 3.9%, with a distribution similar to that of silt.

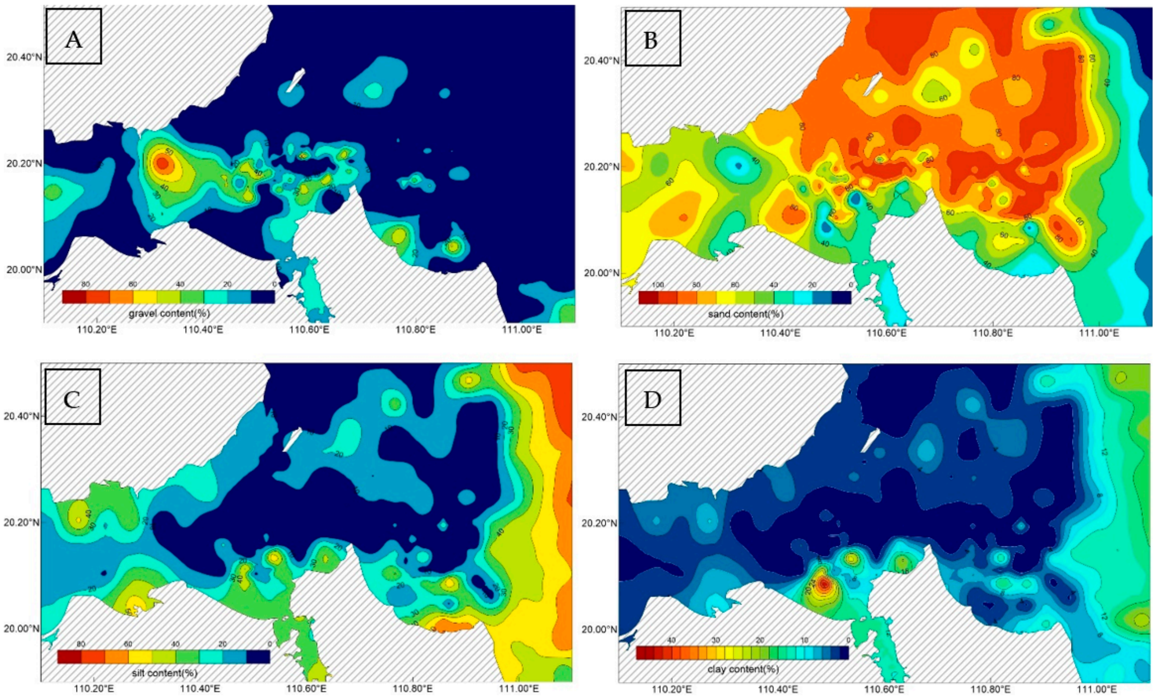

Figure 2. Distribution of sediment components percentage, (**A**) gravel, with contour interval of 10%, (**B**) sand, with contour interval of 10%, (**C**) silt, with contour interval of 10%, and (**D**) clay, with contour interval of 2%.

The distribution of sediment components reflects the hydrodynamics. The gravel sediments are mainly located inside the strait, mostly along the eroded channel; the finer particles are eroded away by the east-west reciprocating tidal current and the gravel component remains. Over the tidal sand ridges, as the current velocity decreases gradually from west to east, more sandy and muddy sediments are deposited, resulting in the distribution of fine-grained sediment shown in Figure 3. The grain size of the sediments in the study area ranges from −1.15 φ to 8.07 φ, with an average value of 2.15 φ. The grain size range in the tidal ridges is between −1 φ and 2 φ, classified as coarse sand. The grain size range in the muddy zone is between 4 φ and 6 φ, classified as coarse silt. The sorting coefficient in the study area is 0.40–4.27, with an average value of 1.69, indicating poor sorting. In the tidal ridges, the sorting coefficient is relatively low, indicating that the sediment is transported over long distances. The tidal ridge area is an important sediment transport and aggregation area. In general, the distribution characteristics of mean grain size and sorting correlate well with the orientation of the tidal sand ridges.

3.2. Critical Incipient Velocity

Figure 4 shows the distribution of critical incipient velocity at 100 cm above the sea bed ($U_{100\ cr}$) as a contour map. The $U_{100\ cr}$ of the study area is between 0.124 and 0.792 m·s^{-1} with an average value of 0.437 m·s^{-1}. High $U_{100\ cr}$ corresponds to the coarse sediments of the study area. The $U_{100\ cr}$ from the Qiongzhou Strait to the Southwest Shoal is higher than average, exceeding 0.5 m·s^{-1} in all, and exceeding 0.6 m·s^{-1} in some cases. East of Hainan Cape, where the sediment type is fine sand, the $U_{100\ cr}$ is mostly between 0.4~0.5 m·s^{-1}. In other areas covered by muddy sediments, the $U_{100\ cr}$ is less than 0.3 m·s^{-1}. This spatial distribution of critical incipient velocity leads to large variation of sediment erodibility time, hence the stability of the sandy seabed during the tide cycle.

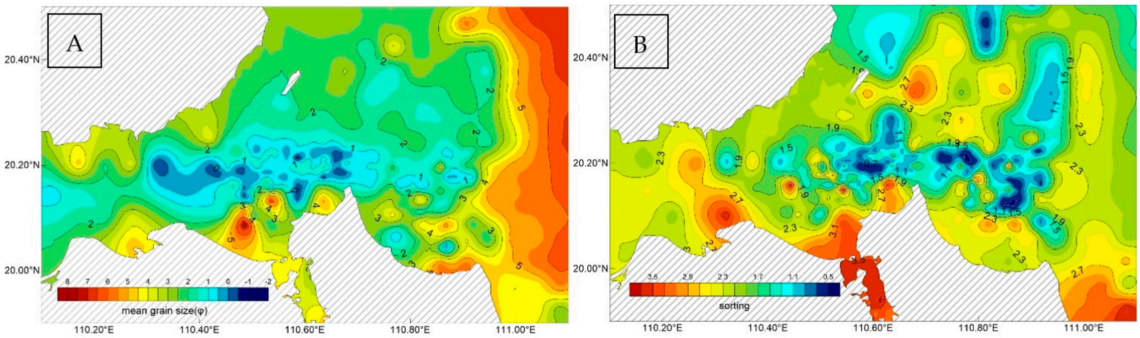

Figure 3. Distribution of grain size parameters, (**A**) mean grain size contours with an interval of 0.5 phi, (**B**) sorting contours with an interval of 0.2.

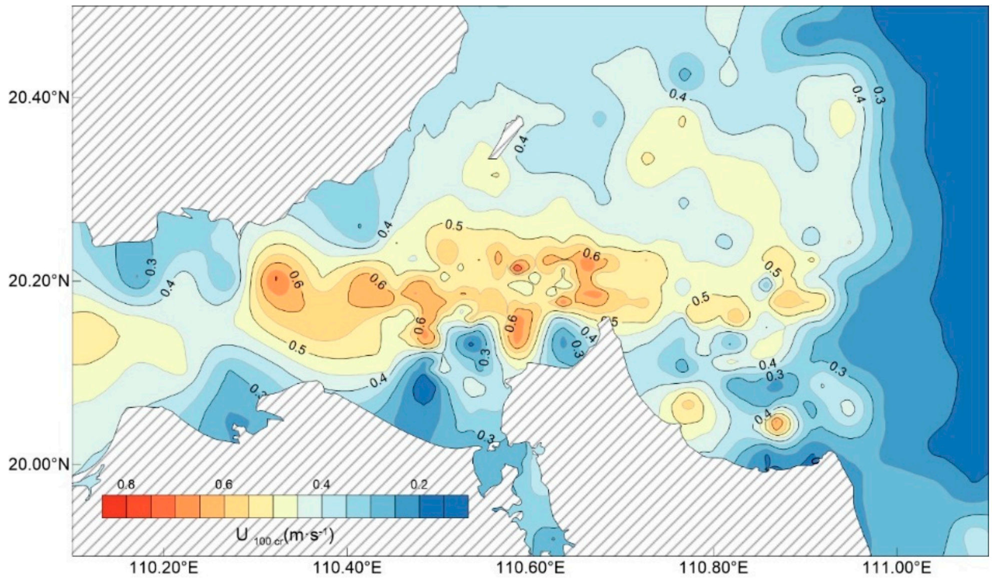

Figure 4. Contour map of critical incipient velocity 100 cm above the seabed.

3.3. Temporal and Spatial Characteristics of Tidal Currents

Characteristics of the irregular semi-diurnal tides were clearly identified based on the tidal current data from the six observation stations. The tidal current is an east-west reciprocating current that manifests in four phases: ebb with eastward current, flood with westward current, ebb with westward current, and flood with eastward current [4,34]. The current velocity was about 1.0 m·s^{-1} at flood tide and between 0.2~0.8 m·s^{-1} at ebb tide. The eastward current had a smaller tide range, higher flood current velocity, and shorter flood tide duration than the westward current. The maximum current velocity occurred near Hainan Cape (Station C1) during the flood tide, and the minimum current velocity occurred during the current reversal period of ebb tide (as shown in Figure 5).

As shown in Figure 6, the tidal current was stronger at stations C1, C3, and C5 (located in the outer sea area) than at stations C2, C4, and C6 (located in the coastal waters). Station C1 had the greatest velocity (with maximum up to 2.0 m·s^{-1}). At these stations, the eastward current velocity was significantly greater than the westward velocity. Because of the topography, the current direction at each station shows some variability, but the directions of flood and ebb tide are essentially consistent with the depth contours (as shown in Figure 6).

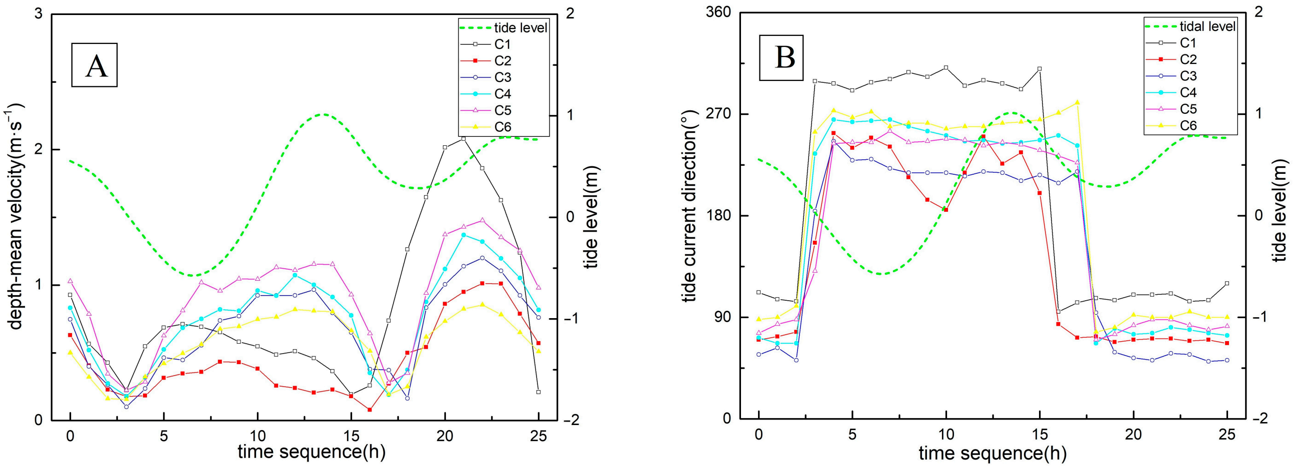

Figure 5. Time series of the tidal current at the six observation stations during spring tide. The green line represents the tidal level. (**A**) depth-mean velocity curve during one tidal period. (**B**) tidal current direction curve during one tidal period.

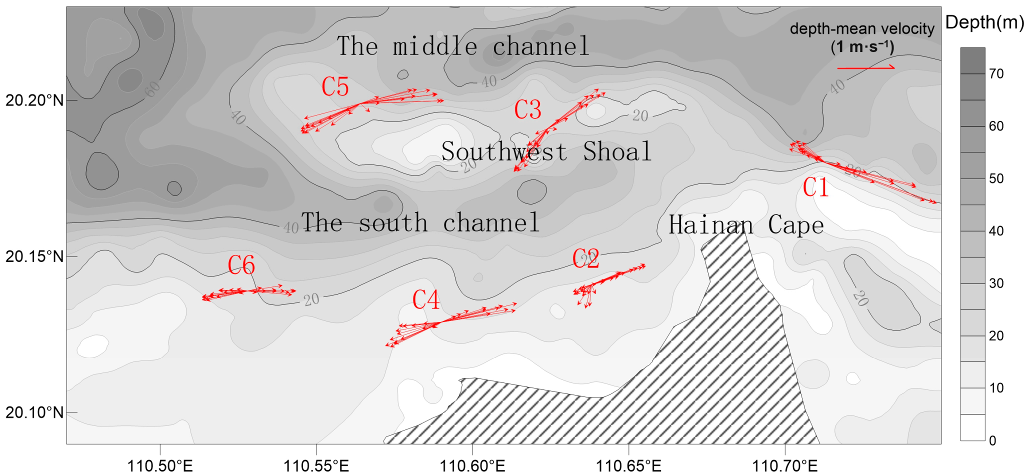

Figure 6. Tidal ellipse of the depth-mean velocity and direction of the tidal current at the six observed stations. The red arrow points in the tidal current direction, while the length of the arrow line indicates the magnitude of the current velocity.

The numerical simulation of the tidal current field is in good agreement with data from the observation stations. Four typical phases of the tidal current field are shown in Figure 7.

The intensity of the westward current was greater than that of the eastward current, especially in the north and middle of the strait. In flood, the depth-mean velocity of westward current was as high as an average value of 0.93 m·s^{-1}. The velocity reached up to 1.30 m·s^{-1} in the northern part of the Qiongzhou Strait and in the shoal area, which accounts for about 40% of the study area. At ebb tide, the current velocity increased, especially in the middle of the Qiongzhou Strait, where the current velocity averaged 1.54 m·s^{-1} (see Table 1 for details). The highest velocities for the eastward current occurred in the southern part of the Qiongzhou Strait and some of the shoal areas. The eastward ebb current ran along the middle and south channels, Southwest Shoal, North Shoal, and South Shoal. The highest velocities for the eastward flood current occurred mainly in the Wailuo Channel and along the coast of Hainan Island. Therefore, the central and northern parts of the Qiongzhou Strait were strongly influenced by the westward currents, while the eastward currents strongly influenced the south and coastal areas of Hainan Island. The main reason for this is the effect of the coastal currents in western Guangdong, which make the waters of the Qiongzhou Strait show a westward transportation trend. In the southern parts of the Qiongzhou Strait, the effect is not quite as obvious due to blockage by the Hainan Island coast, which results in relatively strong eastward currents [40,54].

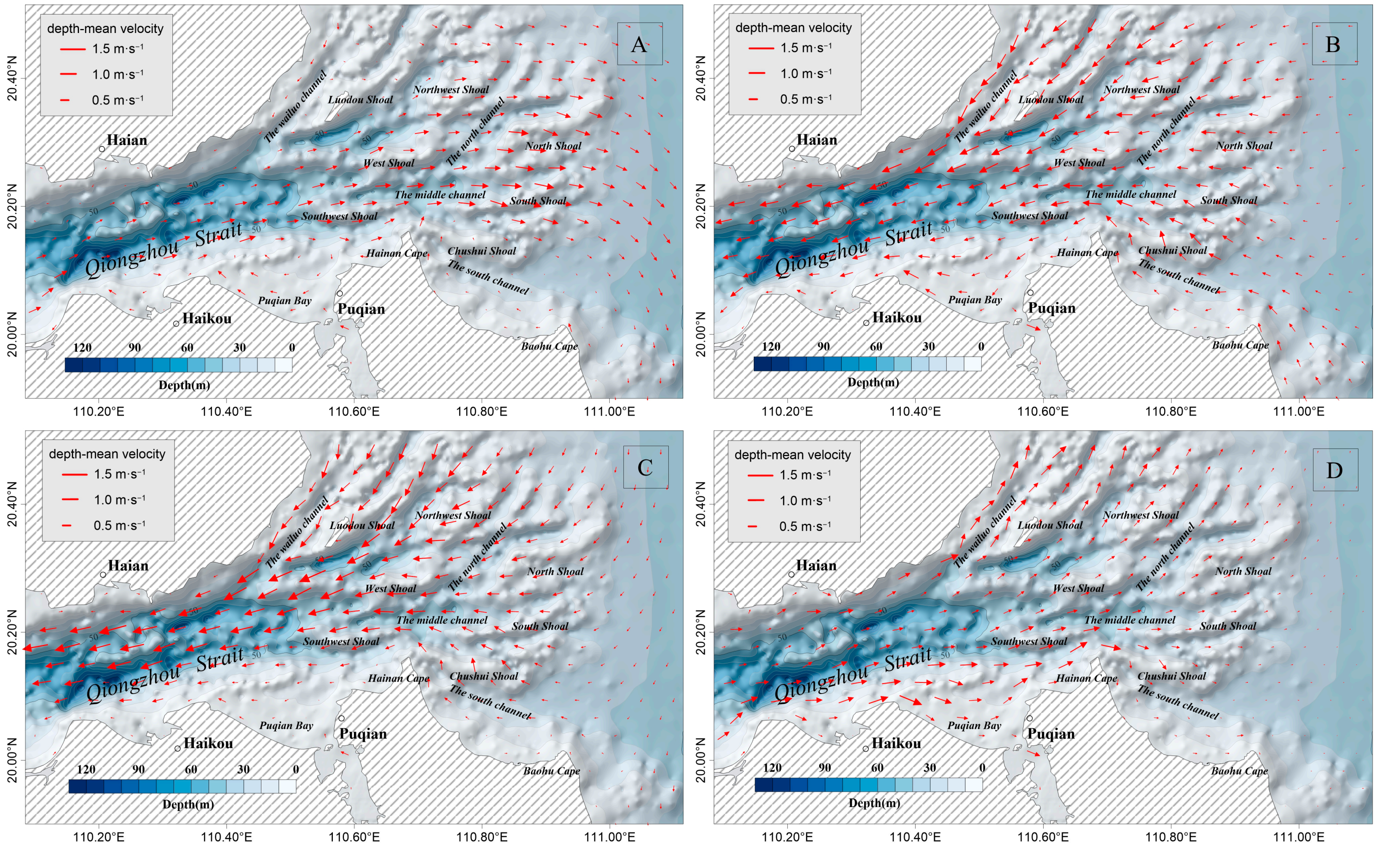

Figure 7. Characteristics of the tidal current field at the east entrance of the Qiongzhou Strait during different tidal phases. (**A**) Eastward ebb current, (**B**) westward flood current, (**C**) westward ebb current, and (**D**) eastward flood current.

Table 1. The tidal current velocity in different tide phases at the east entrance of the Qiongzhou Strait. Phase A represents ebb with an eastward current. Phase B represents flood with a westward current. Phase C represents ebb with a westward current. Phase D represents flood with an eastward current. The number before the slash shows the maximum velocity and the number behind the slash shows the average velocity, with unit of m·s^{-1}. The number in the bracket shows the distribution proportion of the statistical scope.

Location	**The Tide Phases**			
	Phase A	**Phase B**	**Phase C**	**Phase D**
The whole Study area	1.96/0.67	2.30/0.93	2.72/0.92	2.57/0.67
Inside the strait and the shoal area	1.96/0.92(31%)	2.30/1.30(40%)	2.72/1.59(34%)	2.57/1.24(17%)
Other areas	1.10/0.32(69%)	2.20/0.54(60%)	2.02/0.59(66%)	2.00/0.55(83%)

3.4. Analysis of Bedload Transport Rate

Figure 8 shows the bedload transport rates calculated from data on the grain size and tidal currents during the four tidal phases. About 60–90% of the sediments in the study area have been transported. The eastward and westward currents can transport about 60–65% and 75–90% of the sediments, respectively. This indicates that sediments in the study area have been substantially disturbed by tidal currents. Therefore, the possibility of sediment transport is relatively high. In the central part of the Qiongzhou Strait, there is evidence of strong erosion of the original strata, whereas at the eastern entrance of the Strait, there is evidence of instability and migration of sand ridges [6,55].

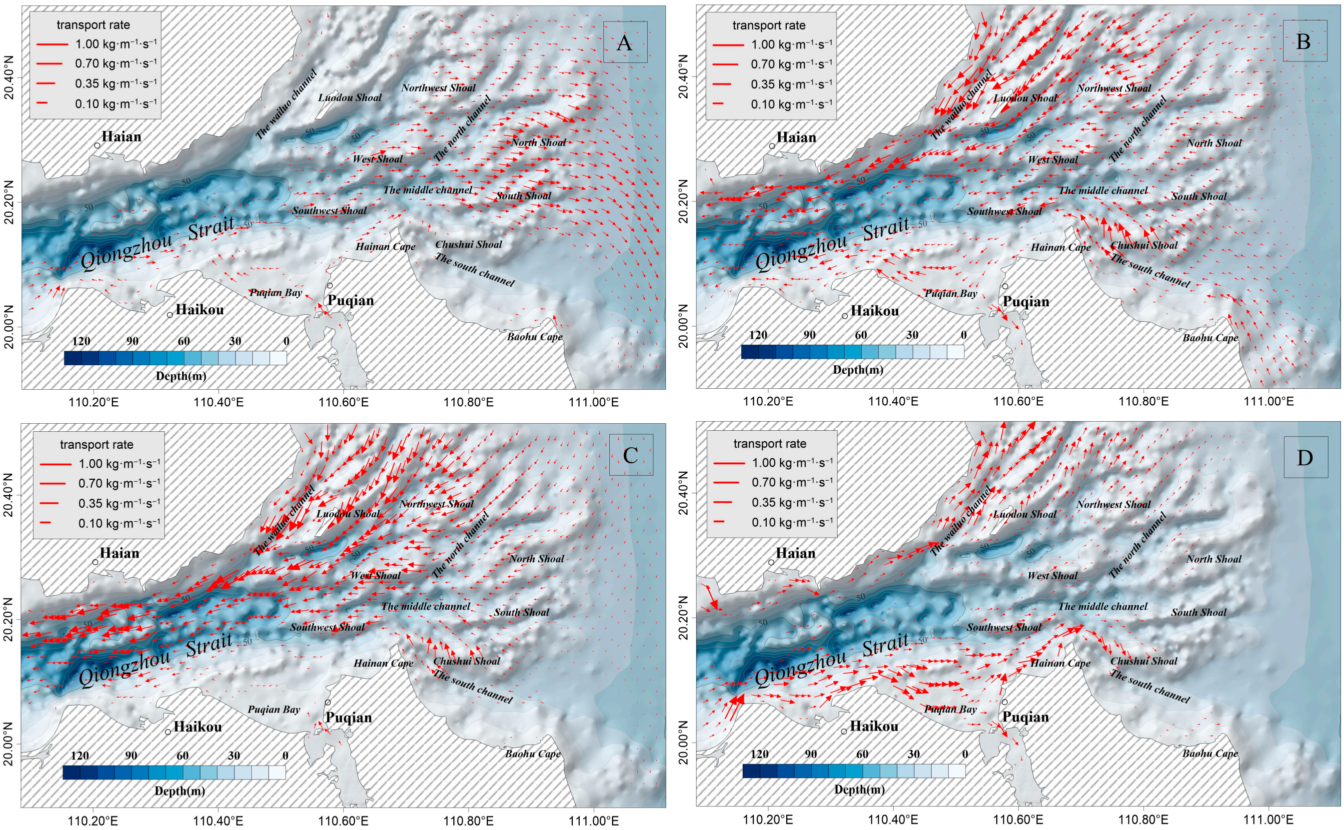

Figure 8. Characteristics of bedload transport rate at the east entrance of the Qiongzhou Strait during different tidal phases. (**A**) Eastward ebb current, (**B**) westward flood current, (**C**) westward ebb current, (**D**) eastward flood current.

The distribution of transport rate shows that high values of q_b are concentrated in the northern and southern parts of the Qiongzhou Strait, as well as in the shoal areas. In the central parts of the Strait, where the sediments have been sorted by high-speed currents within the channels for a long time, the in situ gravels are too coarse to be easily carried away, which results in a low transport rate. In the northern parts of the Qiongzhou Strait, the effect of strong westward currents results in sediments being transported at a rapid rate (0.12–0.16 kg·m^{-1}·s^{-1}) in a southwest direction along the Luodou Shoal, Northwest Shoal, West Shoal, and the nearby channels. In the southern parts of the Strait, where water depths are less than 50 m, eastward flood currents transport sediments to the Chushui Shoal at an average rate of 0.12 kg·m^{-1}·s^{-1}. During the ebb period associated with eastward currents, the high values of q_b are transferred to the South Shoal and the North Shoal. As a result, the average q_b is 0.08 kg·m^{-1}·s^{-1}.

During spring tide, sediment transport mainly occurs along the northern and southern parts of the Qiongzhou Strait, at water depths between 10 and 50 m. The transport rate is significantly greater in the north than in the south. The net transport direction is westward in the north and eastward in the south. The eastward transport peaks during flood tide. The transport rate is weaker in the central parts of the strait, lower by one to two orders of magnitude. This finding is similar to the results of previous studies [4,5,16]. In the shoal area, the transport rate is consistently high during the spring tide period, indicating the strong influence of the ridges. However, the transport rate and direction on both sides of the middle channel and the north channel are quite different [5].

It is estimated that the net bedload transport in the study area mainly occurs in the northern, southern, and shoal areas of the Qiongzhou Strait, and the main channel has a low net bedload transport flux (Figure 9). In the northern part of the strait, the net bedload transport direction is westward, while in the southern part of the strait and the shoal area, the net bedload transport direction is eastward, but only in the bay on the southern coastline (such as Puqian Bay, the south channel, etc.) is the net bedload transport direction westward (as shown in Figure 9). This trend correlates the intensity of the tidal current, demonstrating that the east-west tidal current is the primary influence on bedload in the Qiongzhou Strait.

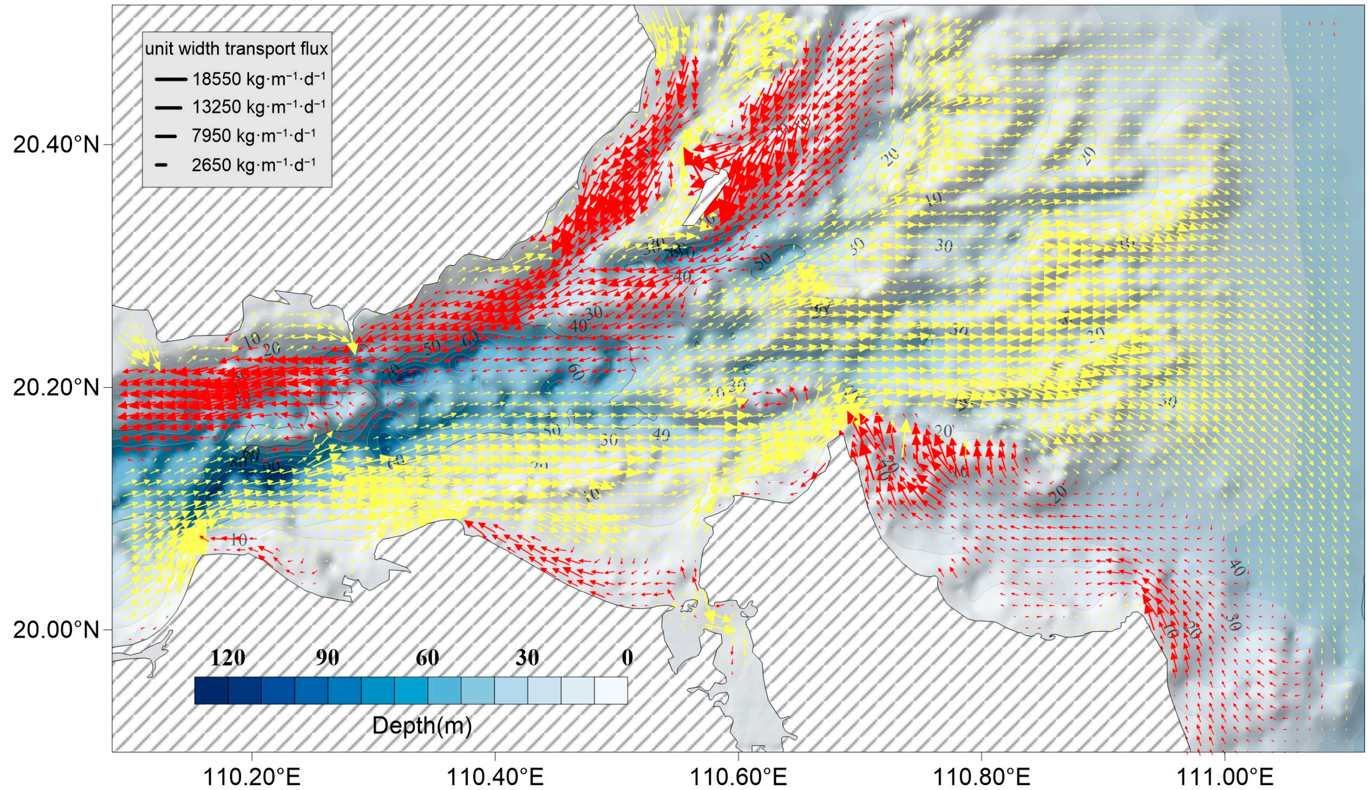

Figure 9. Net bedload transport flux at the east entrance of Qiongzhou Strait during spring tide. The yellow arrow indicates that bedload transport is eastward and the red arrow indicates that bedload transport is westward.

3.5. Estimation of Bedload Transport Flux

Figure 10 shows the transport rate at six observation stations near the Southwest Shoal. The bedload transport rate in the southern part of the study area was generally high, indicating that the sediments were quite active. Sediment movement occurred during flood tide. The transport rate was significantly greater moving eastward than westward, which is similar to the simulation results. The relatively higher rates at stations C1 and C2 occurred during flood tide when the currents were eastward. Through the calculation from the observed data of six stations, the maximum values were 0.436 $kg{\cdot}m^{-1}{\cdot}s^{-1}$ and 0.269 $kg{\cdot}m^{-1}{\cdot}s^{-1}$ in the directions of 110° and 70° for station C1 and C2, respectively. During the rest of the field observation, no transport occurred at station C1, and the transport rate at station C2 was SWS at 10^{-2} $kg{\cdot}m^{-1}{\cdot}s^{-1}$. At other stations, the transport rates were mostly less than 0.10 $kg{\cdot}m^{-1}{\cdot}s^{-1}$, with directions of 80–90° and 250–260°. At station C3, the transport direction was 50° and 220°. For the six observed stations in the southern part of the study area, the U_{100} was mostly greater than $U_{100\,cr}$ during the spring tide period, especially when the current direction was eastward. These conditions resulted in a large near-bed shear stress, which moved the sediments. In contrast, the westward U_{100}

was close to or slightly higher than the $U_{100\ cr}$. As a result, at some stations (such as C1 and C4), sediments would not move obviously. The simulated result also shows (Figure 9) that from the Southwest Shoal to Hainan Cape, the net bedload transport direction is eastward, which is roughly the same as the observed stations.

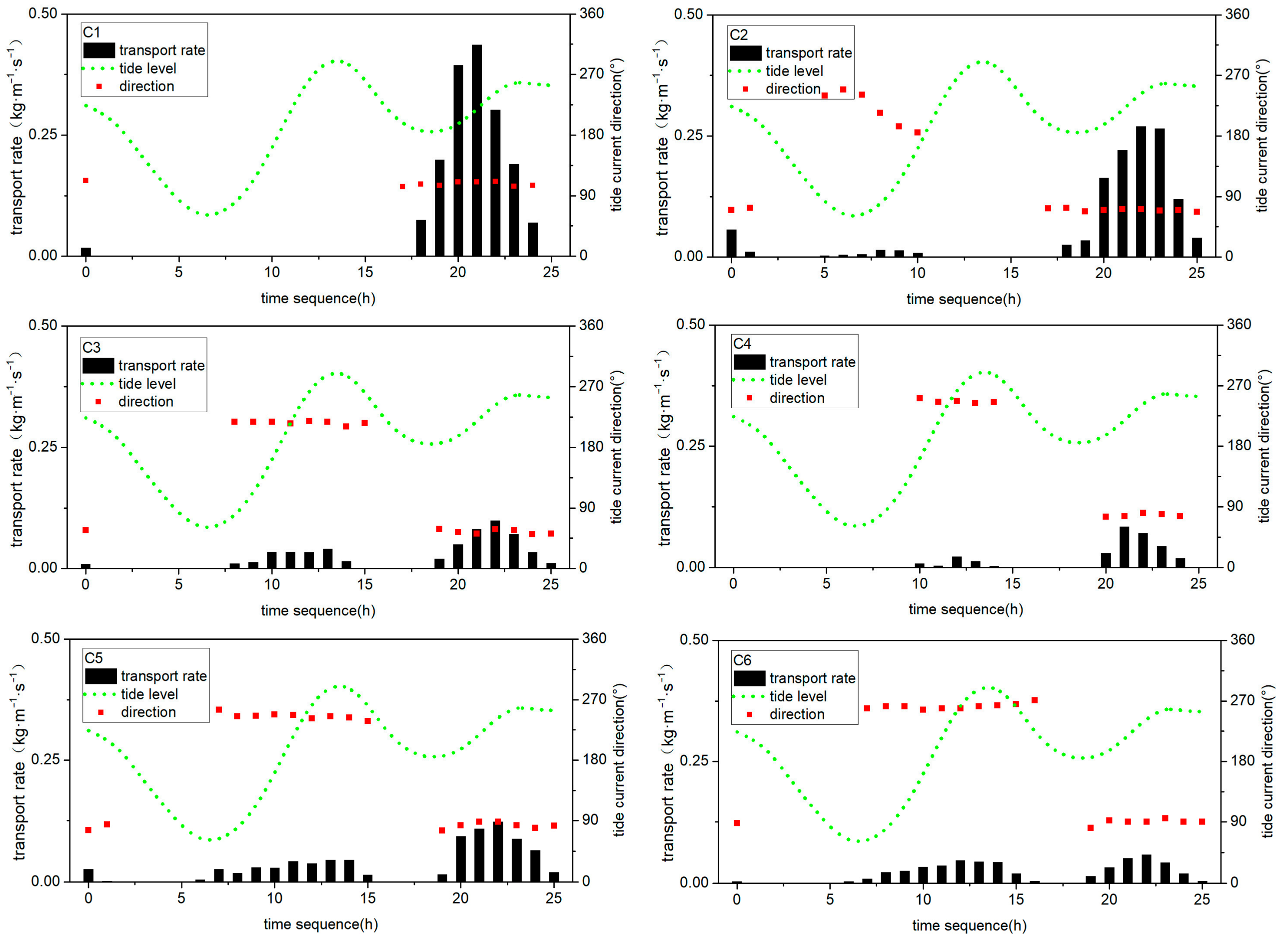

Figure 10. Time sequence diagrams of sediment transport rates at the six observed stations. The green line represents the tidal level. The red point represents the tidal current direction. The black bar shows the bedload transport rate.

Table 2 displays the bedload transport flux obtained by decomposing the transport rate vector into two directions, north and east, and then calculating their integrations over 25 h. Stations C1 and C2 have the largest transport fluxes, 6048.5 $kg \cdot m^{-1} \cdot d^{-1}$ and 4061.8 $kg \cdot m^{-1} \cdot d^{-1}$, respectively, both in an eastward direction and parallel to the depth contours. The transport flux at other stations is slightly less than 1000 $kg \cdot m^{-1} \cdot d^{-1}$ in an eastward direction. The transport flux at station C6 is only 279.6 $kg \cdot m^{-1} \cdot d^{-1}$ in a WWS direction.

Table 2. The unit width bedload transport flux at the observation stations.

Station Name	Mass Unit Width Transport Flux ($kg \cdot m^{-1} \cdot d^{-1}$)	Volume Unit Width Transport Flux ($m^3 \cdot m^{-1} \cdot d^{-1}$)	Direction (°)
C1	6048.5	2.28	109
C2	4061.8	1.53	72
C3	716.0	0.27	72
C4	719.3	0.27	80
C5	938.7	0.35	105
C6	279.6	0.11	233

Through simulation, the average net bedload transport flux in the study area is 5873.8 kg·m^{-1}·d^{-1}, the median is 3411.9 kg·m^{-1}·d^{-1}, the first quartile is 1167.9 kg·m^{-1}·d^{-1}, and the third quartile is 8030.3 kg·m^{-1}·d^{-1}. This indicates that the relative peak value of net bedload transport flux in the study area is relatively large, but the values in most study areas (about 66%) are less than the average value. Therefore, the net bedload transport flux obtained by tidal current simulation seems to be in agreement with the observed stations, but there are some differences. For example, station C6 has a small net transport flux, with quite a difference from the simulation results, which may be related to the effect of longshore drift and waves. This simulation did not consider the influence of waves and longshore drift. Therefore, for the local complex environment, the model needs to be improved so as to simulate the hydrodynamic environment and the sedimentary dynamic process of bedload more effectively.

As shown in Figure 9, the transport of bedload in the study area presents the characteristics of the center to the east and the two sides of the channel to the west, but the sediment flux in the two directions is quite different. According to calculations, the distribution area of eastward bedload transport is 114% higher than that of westward, and the average mass unit width transport flux is 12% higher than that of westward. Therefore, the bedload transport trend in the study area is generally eastward, which is mainly distributed in the south of the Strait and the shoal area.

In general, the sediment transport process in the study area is complicated, with bedload transport rates that vary substantially across time and space. Bedload transport is controlled mainly by the reciprocating current in the strait, as well as by sediment sources. Studies have shown that the sediment sources are diverse in the study area, including the erosion of the central parts of the strait, the input of terrigenous materials by rivers, and the materials from the northern shelf of the South China Sea, leading to large differences in the characteristics of the sedimentary environment [55–57]. In gravelly deposit zones, sediment transportation is weak, although the current velocity is high during spring tide. In central parts of the Qiongzhou Strait, a large amount of material was eroded from the original strata during the Holocene, and fine-grained sediments were carried away. The gravelly component was retained, forming a protective layer that prevents further erosion by currents [6,55,56]. Our study found that the main bedload transport channels along the northern and southern coastal zone are characterized by strong tidal currents and fine-grain sediments, which is consistent with other studies [39,58]. Therefore, it is the differences in bedform and sea-land patterns that cause large differences in the form, distance, speed, and direction of bedload transport, further resulting in great variations in seabed stability and bedform [5].

4. Conclusions

The hydrodynamic processes in the Qiongzhou Strait are controlled by the area's topography and the east-west reciprocating tidal currents. Large tidal sand ridges have been formed at the eastern entrance with sand content up to more than 50%. The central parts of the strait are heavily eroded, leaving residual gravel that makes up between 20% and 50% of the sediments. The trend of grain size getting finer from the west to east indicates that the sediments have been transported over a long distance, resulting in well-sorted sediments over the sand ridges.

The tide at the eastern entrance of the Qiongzhou Strait is influenced by tidal waves from the South China Sea and the Beibu Gulf, resulting in an irregular semi-diurnal tide. The tidal cycle consists of four phases, including an eastward ebb current, a westward flood current, a westward ebb current, and an eastward flood current. In general, the velocity of the westward current is significantly greater than that of the eastward current, especially in the central-northern parts of the Qiongzhou Strait. The average current velocity during spring tide is between 0.67–0.93 m·s^{-1}. The maximum current velocity is 2.72 m·s^{-1}, which is capable of disturbing 60–90% of the sediments. The bedload transport rate to the west in the northern parts of the strait is 0.12–0.16 kg·m^{-1}·s^{-1}, with a spatial pattern similar to that of tidal currents. In the southern parts of the strait, the bedload is transported mainly eastward, particularly during flood tide, at an average transport rate of 0.12 $kg \cdot m^{-1} \cdot s^{-1}$. Our analysis is consistent with previous observations at the cross section at the central part of the Qiongzhou Strait.

Calculations based on both observational and simulated data present that the bedload transport fluxes are 4061.8–6048.5 $kg \cdot m^{-1} \cdot d^{-1}$ in an eastward direction in the vicinity of the Southwest Shoal. The assessment of morphodynamic stability, the viability of marine engineering, and the evaluation of marine sand resources would all be significantly challenged by such a strong bedload transport rate during spring tide. In order to investigate the function of waves, severe occurrences like typhoons, and the changing climate, we propose that further research be conducted from a more comprehensive perspective.

Author Contributions: Conceptualization, C.T. and X.W. (Xiangbai Wu); methodology, C.T.; analysis, C.T.; investigation, X.W. (Xiangbai Wu); resources, X.W. (Xuemu Wang); data curation, X.W. (Xuemu Wang); writing—original draft preparation, C.T.; writing—review and editing, M.Q. and X.W. (Xiangbai Wu); funding acquisition, C.T. All authors have read and agreed to the published version of the manuscript.

Funding: This research was funded by the Hainan Provincial Natural Science Foundation of China (No. 422RC800), National Natural Science Foundation of China (No. 42076005), Hainan Key Laboratory of Marine Geological Resources and Environment (No. HNHYDZZYHJKF008), the High-level Talent Program of Basic and Applied Basic Research Programs (Field of Natural Science) in Hainan Province under contract No. 2019RC349; "Investigation and Evaluation of Marine Sand Resources in northern Hainan Island" (No. HZ2015-235) from Hainan Provincial Department of Land and Resources, and "Preliminary Work of Marine Sand Transfer Pilot Project in Southwest Shoal" (T102972.510) of Hainan Geological Bureau.

Data Availability Statement: The source code of SCHISM model can be obtained from: https://github.com/schism-dev (accessed on 2 February 2023). The SRTM15+ topography data is available through: https://www.ncei.noaa.gov/archive/accession/download/150537 (accessed on 2 February 2023). The simulated tidal current data is available through: https://doi.org/10.57760/sciencedb.07222 (accessed on 2 February 2023). Other data presented in this study are available on request from the corresponding author.

Conflicts of Interest: The authors declare no conflict of interest.

References

1. Ye, C.C. Distribution of sediments and submarine topography of Qiongzhou Strait. *Trop. Geogr.* **1986**, *6*, 346–353. (In Chinese with English abstract)
2. Liu, Z.X.; Xia, D.X.; Wang, K.Y. Tidal depositional system and patterns of China's continental shelf. *Oceanol. ET Limnol. Sin.* **1998**, *29*, 141–147. (In Chinese with English abstract)
3. Li, Z.H.; Ke, X.K. Prelimary study on tidally-induced sediment fluxes of the Qiongzhou Strait. *Mar. Sci. Bull.* **2000**, *19*, 42–49. (In Chinese with English abstract)
4. Li, Z.H.; Ke, X.K.; Wang, Q.; Gao, J. Characteristics of water and sediment transport in the Qiongzhou Strait. *Geogr. Res.* **2003**, *22*, 151–159. (In Chinese with English abstract)
5. Cheng, H.; Li, J.; Yin, D.; Li, M.; Wang, B. Nearshore bedform instability in the eastern entrance to the Qiongzhou Strait, South China Sea. *Front. Earth Sci.* **2008**, *2*, 283–291. [CrossRef]
6. Ni, Y.G.; Endler, R.; Xia, Z.; Endler, M.; Harff, J.; Gan, H.; Schulz-Bull, D.E.; Waniek, J.J. The "butterfly delta" system of Qiongzhou Strait: Morphology, seismic stratigraphy and sedimentation. *Mar. Geol.* **2014**, *355*, 361–368. [CrossRef]
7. Zhang, Q.; Wang, P.; Wang, W.; Zhang, Y. Marine sand resources in the Pearl River estuary waters of China. *J. Mar. Syst.* **2010**, *82*, S83–S89. [CrossRef]
8. Ouillon, S. Why and How Do We Study Sediment Transport? Focus on Coastal Zones and Ongoing Methods. *Water* **2018**, *10*, 390. [CrossRef]
9. Conery, I.; Walsh, J.P.; Mallinson, D.; Corbett, D.R. Marine Geology and Sand Resources of the Southern North Carolina Inner Shelf. *Mar. Georesources Geotechnol.* **2022**, *40*, 1084–1107. [CrossRef]
10. Hasiotis, T.; Gazis, I.-Z.; Anastasatou, M.; Manoutsoglou, E.; Velegrakis, A.F.; Kapsimalis, V.; Karditsa, A.; Stamatakis, M. Searching for potential marine sand resources to mitigate beach erosion in island settings. *Mar. Georesources Geotechnol.* **2021**, *39*, 527–542. [CrossRef]
11. Liu, Y.; Zhong, C.; Bai, B.; Zhou, Y. Assessment of government supervision on the loss of sea sand resource in China. *Econ. Res.-Ekon. Istraživanja* **2022**, *35*, 2732–2746. [CrossRef]

12. Liu, Y.; Li, C.; Omar, R.B.; Shi, X.; Zhang, H.; Faiz, N.N. Sediment Sources and Dispersion on the Western Sunda Shelf, Malay Peninsula, Southern South China Sea. *Water* **2021**, *13*, 2823. [CrossRef]
13. Bates, R.; Velegrakis, A.F.; Brand, C.; Collins, M.B.; Nunn, A. Deep Water and Inshore Aggregates Exploitation; Research Report for the Countryside Council of Wales. 1997; 91p.
14. van Lancker, V.R.M.; Bonne, W.; Velegrakis, A.F.; Collins, M.B. Aggregate extraction from tidal sandbanks: Is dredging with nature an option? *Introduction. J. Coast. Res.* **2010**, *51*, 53–61.
15. Tong, C.; Zhang, K.; Chen, F.; Gou, P. The potential evaluation of marine sand resources in the northern sea areas of Hainan Island. *Geol. China* **2020**, *47*, 1567–1575. (In Chinese with English abstract)
16. de Swart, H.E.; Yuan, B. Dynamics of offshore tidal sand ridges, a review. *Environ. Fluid Mech.* **2019**, *19*, 1047–1071. [CrossRef]
17. Khalil, S.M.; Forrest, B.M.; Haywood, E.; Raynie, R.C. Surficial sediment distribution maps for sustainability and ecosystem restoration of coastal Louisiana. *Shore Beach* **2018**, *86*, 21–29.
18. Jia, J.; Wang, Y.P.; Gao, S.; Wang, A.; Li, Z. Interpreting grain-size trends associated with bedload transport on the intertidal flats at Dafeng, central Jiangsu coast. *Chin. Sci. Bull.* **2006**, *51*, 341–351. [CrossRef]
19. Du, X.Q.; Li, Y.; Gao, S. Characteristics of the large-scale sandwaves, tidal flow structure and bedload transport over the Taiwan Bank in southern China. *Acta Oceanol. Sin.* **2008**, *30*, 124–136. (In Chinese with English abstract)
20. Li, D.Y.; Chen, J.; Wang, Y.P.; Wang, A.; Yang, Y. High resolution measurement and analysis of sediment dynamics in bottom boundary layer of macro tidal esturary. *Acta Sedimentol. Sin.* **2014**, *32*, 278–289. (In Chinese with English abstract)
21. Wang, A.J.; Lai, Z.K.; Ye, X.; Wang, L. Sediment transport in Minjiang River estuary and adjacent shelf area and associated resource effect. *Oceanol. ET Limnol. Sin.* **2020**, *51*, 1013–1024. (In Chinese with English abstract)
22. Collins, M.B.; Balson, P.S. Coastal and Shelf Sediment Transport: An Introduction, Coastal and Shelf Sediment Transport. *Geol. Soc. Lond. Spec. Publ.* **2007**, *274*, 1–5. [CrossRef]
23. Folk, R.L. A review of grain size parameters. *Sedimentology* **1966**, *6*, 73–93. [CrossRef]
24. Visher, G.S. Grain size distributions and depositional of processes. *J. Sediment. Petrol.* **1969**, *39*, 1074–1106.
25. Mclaren, P.; Bowles, D. The effects of sediment transport on grain-size distributions. *J. Sediment. Petrol.* **1985**, *55*, 457–470.
26. Gao, S.; Collins, M.; Lanckneus, J.; De Moor, G.; Van Lancker, V. Grain size trends associated with net sediment transport patterns: An example from the Belgian continental shelf. *Mar. Geol.* **1994**, *121*, 171–185. [CrossRef]
27. Zanke, U.; Roland, A. Sediment Bed-Load Transport: A Standardized Notation. *Geosciences* **2020**, *10*, 368. [CrossRef]
28. Kalra, T.S.; Suttles, S.E.; Sherwood, C.R.; Warner, J.C.; Aretxabaleta, A.L.; Leavitt, G.R. Shoaling Wave Shape Estimates from Field Observations and Derived Bedload Sediment Rates. *J. Mar. Sci. Eng.* **2022**, *10*, 223. [CrossRef]
29. Soulsby, R.L.; Damgaard, J.S. Bedload sediment transport in coastal waters. *Coast. Eng.* **2005**, *52*, 673–689. [CrossRef]
30. Wang, W.J. Propagation of tidal waves and development of sea-bottom sand ridges and sand ripples in northern South China Sea. *Trop. Oceanol.* **2000**, *19*, 1–7. (In Chinese with English abstract)
31. Duffy, G.; Clarke, H.J.E. Measurement of Bedload Transport in a Coastal Sea Using Serial Multibeam Surveying: Assessing bedload formulae using sand dune migration. In *IAS Special Publication # 44, Sediments, Morphology and Sedimentary Processes on Continental Shelves*; Wiley: Hoboken, NJ, USA, 2012; pp. 249–272.
32. Krabbendam, J.M.; Roche, M.; Van Lancker, V.R.; Nnafie, A.; Terseleer, N.; Degrendele, K.; De Swart, H.E. Do tidal sand waves always regenerate after dredging? *Mar. Geol.* **2022**, *451*, 106866. [CrossRef]
33. Wang, S.; Toumi, R. Recent migration of tropical cyclones toward coasts. *Science* **2021**, *371*, 514–517. [CrossRef]
34. Zou, Q.; Xie, D. Tide-surge and wave interaction in the Gulf of Maine during an extratropical storm. *Ocean. Dyn.* **2016**, *66*, 1715–1732. [CrossRef]
35. Xie, D.; Zou, Q.; Cannon, J.W. Application of SWAN+ADCIRC to tide-surge and wave simulation in Gulf of Maine during Patriot's Day storm. *Water Sci. Eng.* **2016**, *9*, 33–41. [CrossRef]
36. Kuang, C.; Han, X.; Zhang, J.; Zou, Q.; Dong, B. Morphodynamic Evolution of a Nourished Beach with Artificial Sandbars: Field Observations and Numerical Modeling. *J. Mar. Sci. Eng.* **2021**, *9*, 245. [CrossRef]
37. Chen, L.; Zhang, Y.; Li, T.; Yang, W.; Chen, J. Sedimentary environment and its evolution of Qiongzhou Strait and nearby seas since last ten thousand years. *Earth Sci.—J. China Univ. Geosci.* **2014**, *39*, 696–704. (In Chinese with English abstract)
38. Shi, M.; Chen, C.; Xu, Q.; Lin, H.; Liu, G.; Wang, H.; Wang, F.; Yan, J. The role of the Qiongzhou Strait in the seasonal variation of the South China Sea Circulation. *J. Phys. Oceanogr.* **2002**, *32*, 103–121. [CrossRef]
39. Chen, C.; Li, P.; Shi, M.; Zuo, J.; Chen, M.; Sun, H. Numerical study of the tides and residual currents in the Qiongzhou Strait. *Chin. J. Oceanol. Limnol.* **2009**, *27*, 931–942. [CrossRef]
40. Shi, M.C. Study comments on circulation of Beibu Gulf. *Guangxi Sci.* **2014**, *21*, 313–324. (In Chinese with English abstract)
41. Wang, Q.; Wang, X.; Xie, L.; Shang, Q.; Lu, Y. Observed water current and transport through Qiongzhou Strait during August 2010. *Chin. J. Oceanol. Limnol.* **2014**, *32*, 703–708. [CrossRef]
42. Bai, P.; Ling, Z.; Liu, C.; Wu, J.; Xie, L. Effects of tidal currents on winter wind waves in the Qiongzhou Strait: A numerical study. *Acta Oceanol. Sin.* **2020**, *39*, 33–43. [CrossRef]
43. Zhang, Y.; Baptista, A.M. SELFE: A semi-implicit Eulerian-Lagrangian finite-element model for cross-scale ocean circulation. *Ocean. Model.* **2008**, *21*, 71–96. [CrossRef]
44. Zhang, Y.; Ye, F.; Stanev, E.V.; Grashorn, S. Seamless cross-scale modeling with SCHISM. *Ocean Model.* **2016**, *102*, 64–81. [CrossRef]

45. Rosa, J.; Silva, P.A.; Bertin, X.; Fortunato, A.B. Waves, wind and tidal forcing on a sandpit morphodynamics. *J. Coast. Res.* **2011**, *SI 64*, 1170–1174.
46. Ye, F.; Zhang, Y.; Wang, H.; Huang, H.; Wang, Z.; Liu, Z.; Li, X. Cross-Scale Baroclinic Simulation of the Effect of Channel Dredging in an Estuarine Setting. *Water* **2018**, *10*, 163. [CrossRef]
47. Tozer, B.; Sandwell, D.T.; Smith, W.H.F.; Olson, C.; Beale, J.R.; Wessel, P. Global bathymetry and topography at 15 arc sec: SRTM15+. *Earth Space Sci.* **2019**, *6*, 1847–1864. [CrossRef]
48. Bagnold, R.A. *An Approach to the Sediment Transport Problem from General Physics*; U.S. Geological Survey Professional Paper; US Government Printing Office: Washington, DC, USA, 1966; Volume 422, pp. 1–37.
49. Hardisty, J. An assessment and calibration of formulations for Bagnold's bedload equation. *J. Sediment. Petrol.* **1983**, *53*, 1007–1010. [CrossRef]
50. Soulsby, R.L. *Dynamics of Marine Sands*; Thomas Telford Services Limited: London, UK, 1997; p. 249.
51. Miller, M.C.; McCave, I.N.; Komar, P.D. Threshold of sediment motion under unidirectional currents. *Sedimentology* **1977**, *24*, 507–527. [CrossRef]
52. Wang, Y.P.; Gao, S. Modification to the Hardisty equation, regarding the relationship between sediment transport rate and particle size. *J. Sediment. Res.* **2001**, *71*, 118–121. [CrossRef]
53. Morales, J.A.; Lozano, C.; Sedrati, M. Calculated Potential Bedload Versus Real Transported Sands along the Guadiana River Estuary (Spain–Portugal). *J. Mar. Sci. Eng.* **2019**, *7*, 393. [CrossRef]
54. Chen, D.S.; Chen, B.; Yan, J.H.; Xu, H.F. The seasonal variation characteristics of residual currents in the Qiongzhou Strait. *Trans. Oceanol. Limnol.* **2006**, *28*, 12–17. (In Chinese with English abstract)
55. Peng, X.C. Geological structure characteristics and cause of formation analyzing in Qiongzhou Strait, South China Sea. *Geol. Res. South China Sea* **2000**, *12*, 44–57. (In Chinese with English abstract)
56. Xu, D.; Chu, F.Y.; Li, J.B.; Yang, H.L.; Chen, L. Transport and deposition of sediment on the shelf off Western Guangdong to Northeastern Hainan. *J. Jilin Univ. Earth Sci. Ed.* **2014**, *44*, 905–917. (In Chinese with English abstract)
57. Tong, C.; Li, G.; Chen, F.; Zhang, K. Geological characteristics and origin of marine sands in the northeast sea off Hainan Island. *Mar. Geol. Front.* **2018**, *34*, 12–19. (In Chinese with English abstract)
58. Kong, J.; Pan, M.; Shen, C.; Hua, G.; Zhao, H. Analysis of the morphological changes and related sediment transport mechanisms of the Baisha Shoal in the Qiongzhou Strait. China. *J. Coast. Res.* **2016**, *32*, 1428–1444. [CrossRef]